UNDERSTANDING AND ANALYSIS OF FOULING BEHAVIOR OF BARE-WIRE HEATING ELEMENTS IN ELECTRIC WATER HEATING

A. Janzen[1] and E. Y. Kenig[2,3]

[1] Stiebel Eltron GmbH & Co. KG, Dr.-Stiebel-Straße 33, 37603 Holzminden, Germany,
E-mail: alexander.janzen@stiebel-eltron.de (corresponding author)
[2] Chair of Fluid Process Engineering, University of Paderborn, Pohlweg 55, 33098 Paderborn, Germany
[3] Gubkin Russian State University of Oil and Gas, Moscow, Russian Federation

ABSTRACT

The aim of the present work is to understand the effects of crystallization fouling on bare-wire heating elements. To carry out the investigations, a unique experimental set-up was developed. It was used to determine the fouling resistance and investigate the local fouling growth over time using optical measuring methods. The fouling resistance was measured for various flowrates. The optical investigations were used to understand the local and temporal fouling growth. Furthermore, they aided in determining the locally deposited fouling thickness over the heating length of the bare-wire heating elements. The morphology of the deposited crystal layers on the bare-wire heating surface was also analyzed to determine their influence on the heat transfer. The findings of this work can be applied for developing enhanced bare-wire heating systems with improved durability to crystallization fouling. The experimental results were used to derive correlations between the fouling mass weight and the flowrate and between the lifetime and the flowrate.

INTRODUCTION

Electric water heating

The electric water-heating industry includes a wide range of applications, e.g., tankless water heaters, hot-water storage tanks, and drinking-water heat pump applications. All these domestic appliances comprise electric heating elements. Many conventional heating elements for electric water heating are based on either a tubular or a bare-wire heating system. However, knowledge of the fouling behavior of electric heating elements is scarce. Such knowledge is necessary for the successful development of design principles for novel heating-element generations.

Bare-wire heating elements are placed directly in the fluid without any electrical insulation between the heating surface and fluid. Therefore, they require a unique type of electrical insulation. The heating elements are placed into a pressure-tested insulated block. The insulation resistance is realized using long and narrow channels in front of and behind the electric heating elements. The resistance depends on the properties of the fluid flowing through the channels and on the channel geometry. Bare-wire heating elements are typically fabricated using a nickel-chromium alloy (NiCr). Fig. 1 shows a bare-wire heating system.
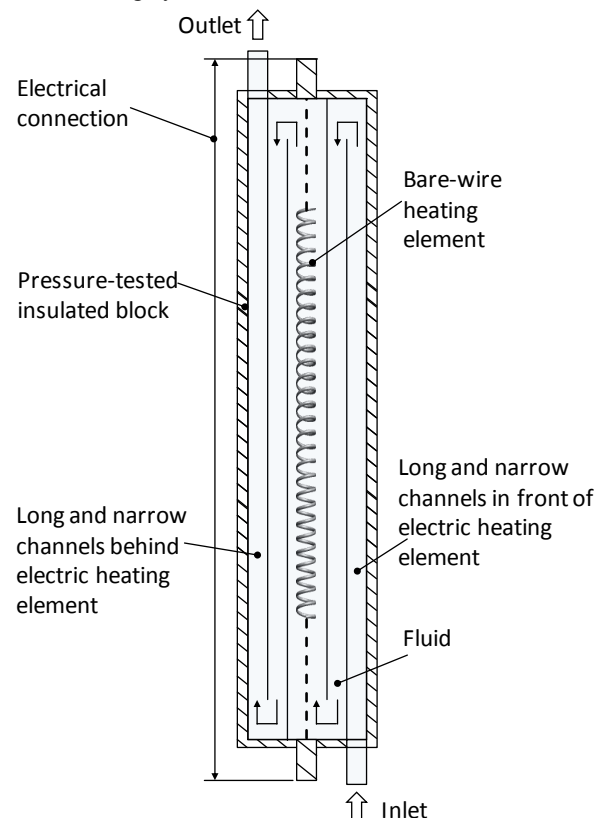
Fig. 1. Schematic of a bare-wire heating system

Bare-wire heating elements are especially suitable for hard-water applications, because they have lower weight and lower surface temperature than conventional tubular heating elements [1]. Owing to the properties of electric bare-wire heating elements, their fouling behavior is characterized by different

stages, which justifies the requirement of a closer investigation.

Crystallization fouling

Crystallization fouling is the deposition of undesirable precipitates on heat-transfer surfaces. According to several investigations [3-7], fouling can cause severe damage to the heat exchanger. In the application field of electric water heating, it is necessary to change the entire heating system when the bare-wire heating elements fail in order to make the device operational again.

The process of crystallization fouling is complex; it begins with nucleation and is followed by crystal growth on the heating surface. The growth of crystals results in a decrease in the overall heat transfer coefficient. If fouling occurs, and if all the operating parameters of the heat exchanging fluid are maintained as constants, the fouling resistance R_f can be determined by

$$R_f = \frac{1}{k_f} - \frac{1}{k_0} \qquad (1)$$

where k_f is the overall heat transfer coefficient for the fouling case and k_0 is the overall heat transfer coefficient for the initial clean condition. The overall heat transfer coefficients are calculated based on the temperature difference between the heating element surface T_s and the fluid T_{fl}. Furthermore, the heat flux $\dot{q}_{el,f}$ at the heating element is used as follows:

$$k_f = \frac{\dot{q}_{el,f}}{T_s - T_{fl}} \qquad (2)$$

The following equation expresses the dependence of the fouling resistance on the temporally changing fouling mass flux:

$$\frac{dR_f}{dt} = \frac{1}{\lambda_f \cdot \rho_f} \cdot J_f \qquad (3)$$

The fouling mass flux J_f is estimated by calculating the difference of two opposing factors, a deposit term and a removal term, as follows:

$$J_f = J_D - J_r \qquad (4)$$

The crystal deposition usually occurs owing to inversely soluble, salts such as $CaCO_3$. The driving force for crystallization fouling is the degree of supersaturation at the heating surface which can be expressed by the saturation index, as reported by Wisotzky [8]. To evaluate a saturated system, the results of a performed tap water analysis are summarized in the ionic activity product. The saturation index is defined as the common logarithm of the ratio of the ionic activity product IAP and the equilibrium solubility product K_L:

$$SI = log\left(\frac{IAP}{K_L}\right) \qquad (5)$$

For a supersaturation of the solution, the saturation index must be greater than zero. The saturation index is used as a measure of the saturation state of a multicomponent test fluid.

EXPERIMENTAL
Fouling experiments

In contrast to other research works [9-11], the fouling tests were performed in a contaminated fluid. For tap water and ground water, the degree of supersaturation can be specified using the saturation index (Eq. 5). The saturation indices of the corresponding mineral phases in the test fluids are calculated using the commercial hydrogeochemical calculation program PHREEQC [12]. To determine the saturation index and the influence of the test fluid, a tap water sample was collected prior and subsequent to each test, followed by a tap water analysis. A total of 60 tap water analyses were evaluated, and their arithmetic mean was used as a reference value for the various tap water components. The saturation index was calculated for the mineral phase $CaCO_3$ (aragonite). For the solution obtained at 12.5 °C, the saturation index for aragonite is 0.13, which indicates a slight supersaturation. Table 1 contains the data obtained from the tap water analysis.

Table 1. Results of tap water analysis

Property / component	Unit	Value
Temperature	[°C]	12.5
pH value	[-]	7.4
Electrical conductivity	[µS/cm, 25 °C]	897.4
Oxygen	[mmol/l]	0.1
Total hardness	[°dH]	29.2
Carbonate hardness	[°dH]	15.0
Hydrogen carbonate	[mmol/l]	5.4
Chloride	[mmol/l]	0.5
Sulfate	[mmol/l]	2.2
Nitrate	[mmol/l]	0.1
Calcium	[mmol/l]	3.0
Magnesium	[mmol/l]	2.4
Sodium	[mmol/l]	0.2
Potassium	[mmol/l]	0.1
SI Aragonite	[-]	0.13
SI Aragonite, $T_f = 60$ °C	[-]	0.71
Pressure	[hPa]	1002.0

An experimental set-up was designed to study the characteristics of the crystallization fouling on bare-wire heating elements as illustrated in Fig. 2. In addition to the measured thermal values, such as surface temperature and inlet and outlet temperatures, the electrical voltage and electrical current were also recorded to determine the electrical power. A variable ratio transformer facilitated the precise adjustment of the corresponding power at the surface. The flow control was adjusted using a variable differential pressure switch with an integrated diaphragm and a Venturi nozzle. A connected upstream tankless

water heater was used to generate a constant inlet temperature of the heating system.
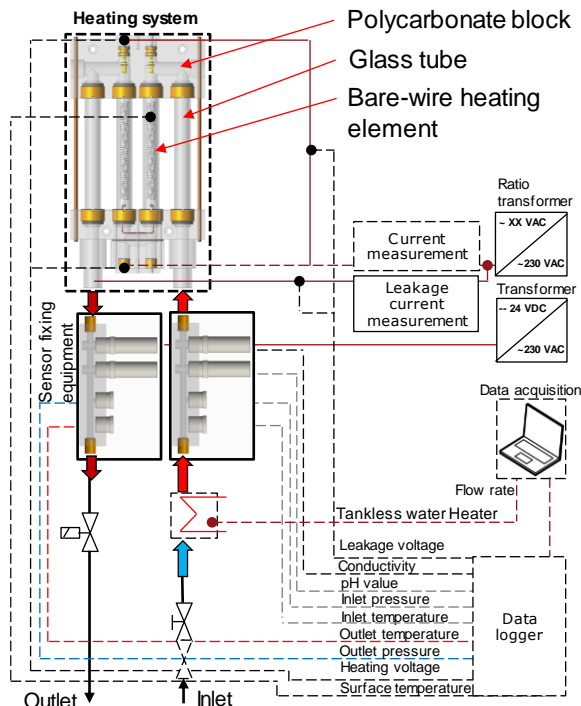
Fig. 2. Schematic of the experimental set-up

Moreover, absolute pressure at the inlet and outlet, electrical conductivity, and pH value were also recorded. The core component of the experimental set-up was the heating system. Inside the glass tube, a specially designed bare-wire heating element was implemented which could reach an electrical power of about 1000 W. Furthermore, in this set-up, one to two heating elements could be installed in series. The technical data of the bare-wire heating element is presented in Table 2.

Table 2. Technical data and geometrical dimensions of a) bare-wire element and b) flow channel

Geometrical shap:	Technical data:		
a)	Electrical power	P_{el}	1000 W
	Electrical voltage	U_N	115 V
	Wire diameter	d_d	400 µm
	Wire lenght	l_{ges}	1446 mm
	Coil lenght	l	100 mm
	Coil pitch	a_w	1.69 mm
	Outside coil diameter	d_w	10 mm
b)	Outside tube diameter	d_a	18 mm
	Inside tube diameter	d_i	16 mm
	Electrical resistivity	ρ_N	0.00011 Ωcm
	Thermal conductivity	λ_{NiCr}	15 W/mK
	Wire surface	A_w	18.16 cm²
	Wire cross-section	A_q	0.00125 cm²
	Tube lenght	l_{tube}	150 mm

The bare-wire surface temperature was measured using a K-type thermocouple as shown in Fig. 3. The thermocouple was adhered to the surface using a ceramic adhesive with a high thermal conductivity to obtain a good thermal contact between the heating surface and thermocouple. Furthermore, it was

important to ensure electrical insulation to the adhesive between the bare-wire heating surface and the thermocouple because of existing electrical potential at the heating surface.
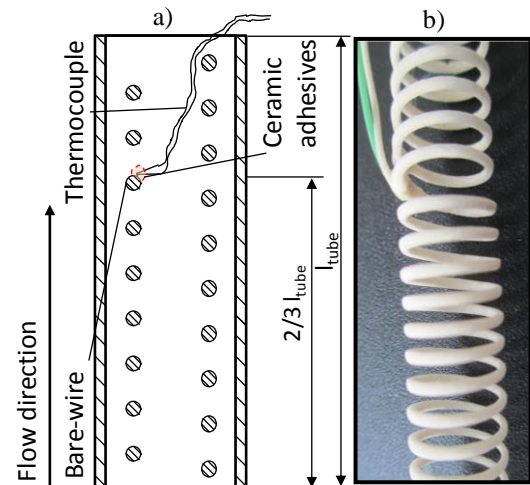
Fig. 3. Fabrication of the bare-wire heating element with thermocouple: schematic of the cross-section (a); bare-wire with a soiled surface (b)

Three fouling experiments were conducted using different flowrates of 2 l/min to 4 l/min. Furthermore, the heat flux was set as 56 W/cm² in all the tests. All the test series were performed until the electric heating elements failed. The aim of these test series was to determine the different fouling durability of the bare-wire heating elements. Table 3 summarizes the test series parameters.

Table 3. Parameters of test series

Tests	Heat flux	Liquid temp.	Flowrate	Reynolds number	Outlet pressure	Saturation index
(NE)	$\dot{q}$ [W/cm²]	T_{fl} [°C]	$\dot{V}$ [l/min]	Re [-]	$p_{t,2}$ [bar]	SI [-]
1	56	45	2	5250	1	1.32
2	56	45	3	7875	1	1.29
3	56	45	4	10500	1	1.30

Optical measuring method

For the optical investigations, all materials in contact with the tap water were fabricated using a glass tube and a transparent polycarbonate block, as shown in Fig. 2. The optical analysis of the local fouling behavior was carried out in six steps.

1. Measuring temporal and local fouling behavior

In front of the experimental set-up, a digital camera was positioned to capture photos of the temporal fouling growth. These images were studied to understand the local fouling growth over time and over the heating length of bare-wire heating elements. Fig. 4 shows a typical fouling curve of bare-wire heating elements along with images of local fouling growth. A discontinuity is observed between a testing time of 18h to 22h. During the test period, parts of the forming crystal deposits were local completely removed or partly peeled off which influence the fouling resistance. The explanation to

the end-life period is given in Section "Results and Discussion".
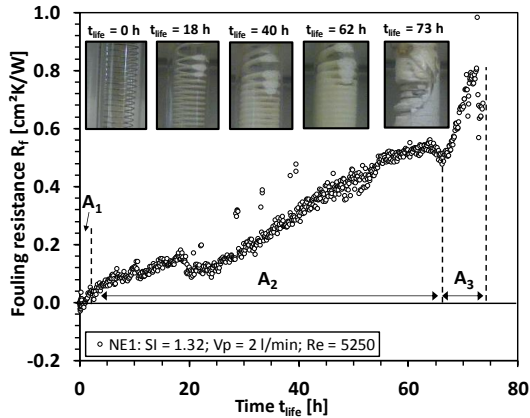
Fig. 4. Fouling curve of the bare-wire heating element for a CaCO$_3$ solution on the test series NE1, A$_1$: Induction period, A$_2$: Crystal growth period, A$_3$: End-life period

2. Preparation of test samples for optical analysis

After the fouling tests, the glass tube with the inserted soiled bare-wire heating element was dismounted to prepare for the optical analysis. In order to minimize the damage to the deposits, the entire tube was encapsulated in a larger polyvinyl chloride tube using a sealing compound, as shown in Fig. 5.
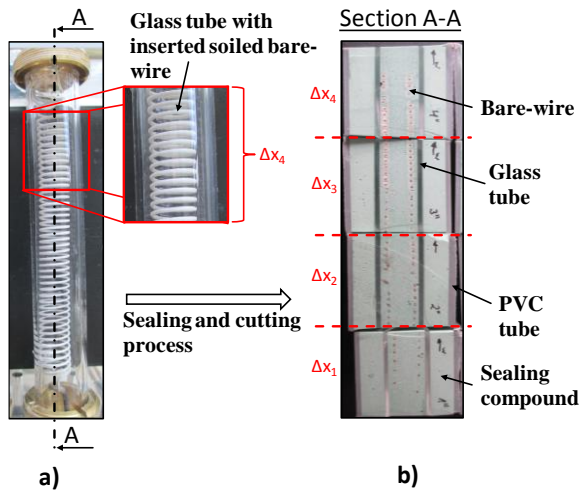
Fig. 5. Illustration of the sealing and cutting process in preparation of the optical analysis: soiled system after fouling test (a); soiled system after the preparation of the test samples for the optical analysis (b)

After the sealing compound has hardened, the prepared tube with the heating element is cut into four segments ($\Delta x_1 - \Delta x_4$) of about 37.5 mm length using a precision saw. Furthermore, each cross segment is cut along the pipe direction (section A–A) as illustrated in Fig. 5b).

3. Optical inspection of final state of CaCO$_3$ deposition

Subsequent to the optical inspection of the final state of the fouling in the prepared test samples, photos were captured of the side section A–A of each cross

segment (Δx_1- Δx_4) using a digital camera. Fig. 6 illustrates the prepared test samples.
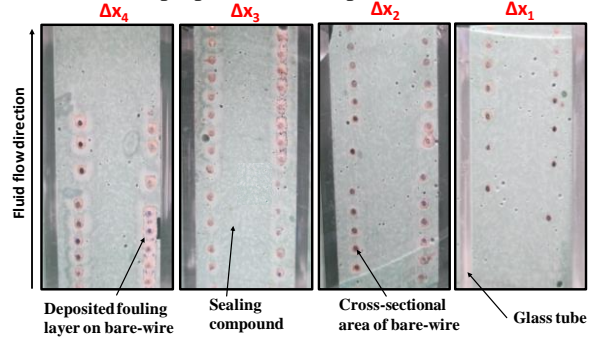
Fig. 6. Test samples of side section A–A of each segment ($\Delta x_1 - \Delta x_4$)

4. Analysis of local fouling layer morphology

The morphology of the contaminated bare-wire heating elements was analyzed using a light microscope. Fig. 7 shows an example of the morphology of the deposited crystals on the bare-wire heating element along with their terminology.
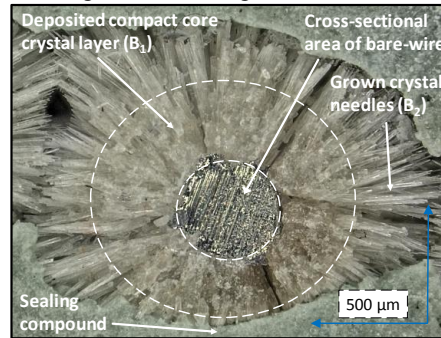
Fig. 7. Local deposited CaCO$_3$ fouling layer on the bare-wire surface (section A–A, segment Δx_3)

5. Determination of deposited fouling layer thickness

The images obtained at step 4 were used to determine the local thickness of the fouling layer on the bare-wire heating elements at each side section A–A using the commercial program ImageJ. Some fouling thicknesses $x_{f,i}$ were measured over the bare-wire circumference as demonstrated in Fig. 8. This procedure was executed for each bare-wire cross-section to determine the fouling thickness over the heating length.
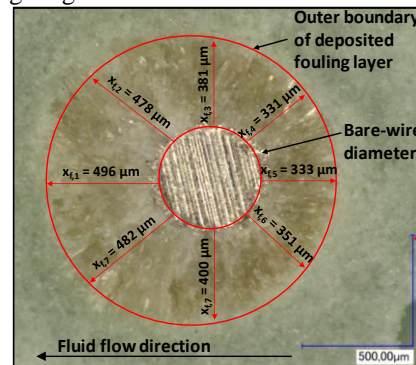
Fig. 8. Measurement of the local fouling thickness at the cross-section of the bare-wire at segment Δx_2

Subsequently, the average layer thickness $x_{f,m,j}$ was calculated using Eq. (6):

$$x_{f,m,j} = \frac{\sum_i^n x_{f,i}}{n} \qquad (6)$$

6. Identification of different stages of local and temporal fouling growth

The images of steps 1, 3, 4, and 5 were used to identify different stages of the local and temporal fouling deposition on the bare-wire heating element. The aim of this procedure is to visualize the fundamental findings regarding the fouling growth on the bare-wire heating elements.

RESULTS AND DISCUSSION
Fouling experiments

Generally, the fouling curve can be subdivided into two major periods: the induction period A_1 and crystal growth period A_2. In the present work, a third period is observed at the end of the fouling curve; this period is called the end-life period A_3, as shown in Fig. 9.
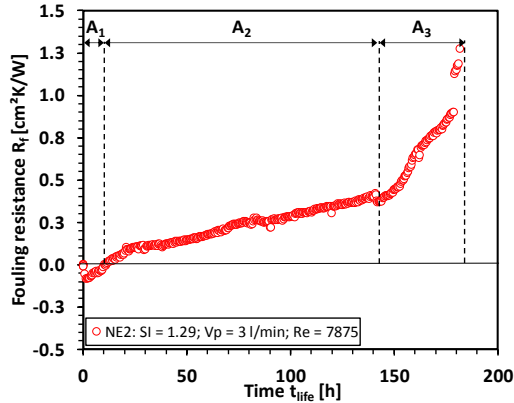
Fig. 9. Typical fouling behavior of the bare-wire heating element in the test series NE2, A_1: Induction period, A_2: Crystal growth period, and A_3: End-life period

An induction period A_1 is visible in many yet not in all the investigated cases. Its occurrence is primarily determined by the molecular and mechanical interactions at the interface between the crystalline deposits and the heat transfer surface. In some cases, the first formed crystals have a positive effect on the heat transfer owing to induced near-wall turbulence [13]. This period is followed by the layer growth period A_2, which is accompanied by a reduction in the heat transfer. In this period, the deposition is mainly driven by the supersaturation of the solution and process conditions. The visible end-life period A_3 is observed after the linear crystal growth period A_2. The main feature of period A_3 is a sudden increase in the fouling resistance as detected in test series NE1 and NE2 (see Fig. 4 and Fig. 9). After the period A_3, the bare-wire heating element fails. An indication of this is a rapid decrease in the heat transfer coefficient. This means that the heating element is not sufficiently cooled, and therefore, the bare-wire has burned through. The influence of various flowrates is shown in Fig. 10; generally, a

reduction in the thermal fouling resistance and induction time is observed as the flowrate is increased, as discussed by Förster [9], Geddert [10], and Albert [14].
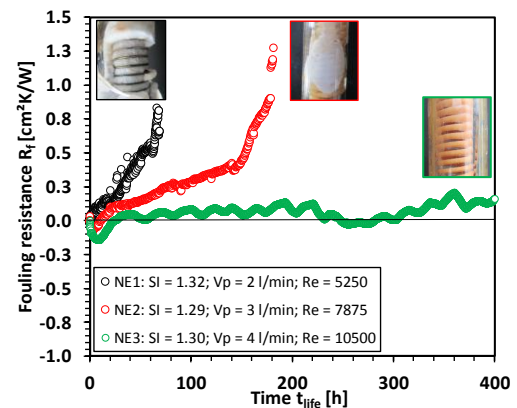
Fig. 10. Fouling resistance R_f for various Reynolds numbers of the bare-wire heating element

When the flowrate is equal to 4 l/min in test series NE3, an interesting fouling behavior is observed. First, a well-formed induction period is distinguished. Second, a saw-tooth course is detected in the layer growth phase. Third, no end-life period is detected. It is observed that with a flowrate of 4 l/min, the bare-wire heating element begins to swing in the flowing fluid. The swinging of the bare-wire increases the turbulence and results in an enhancement in the heat transfer and a reduction in the fouling growth. Therefore, an increase in the fluid flowrate and the swinging of the bare-wire result in two improvements: enhanced removal of deposit crystals and inhibited growth of crystals on the heat transfer surface. Furthermore, no end-life period is detected in test series NE3 because the bare-wire heating element does not fail after 400 h when the test series is completed.

Derivation of correlations

The experimental results were used to derive the correlation between the fouling mass weight and flowrate and between the lifetime and flowrate. Fig. 11 shows the correlation between the fouling mass weight and flowrate.
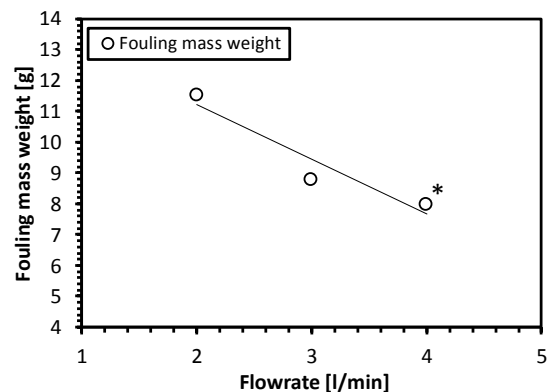
Fig. 11. Correlation between fouling mass weight and flowrate (*The bare-wire heating element has not failed)

The weight of each glass tube with the inserted bare-wire heating element was measured prior and subsequent to the execution of each test series. The fouling mass weight is determined based on the weight increase of the heating elements. The fouling mass weight is reduced when the flowrate is increased. Fig. 12 illustrates the relationship between the lifetime of the bare-wire heating elements and the various flowrates considered. The lifetime raises with an increase in the flowrate.
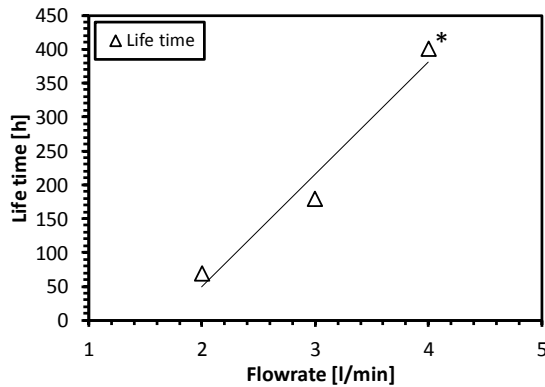
Fig. 12. Correlation between the lifetime and flowrate (*The bare-wire heating element has not failed)

Optical investigations of local fouling behavior

In front of the experimental set-up, a digital camera was used to capture images along the heating length of the bare-wire heating element. Fig. 13 presents the images of test series NE2 at various times.
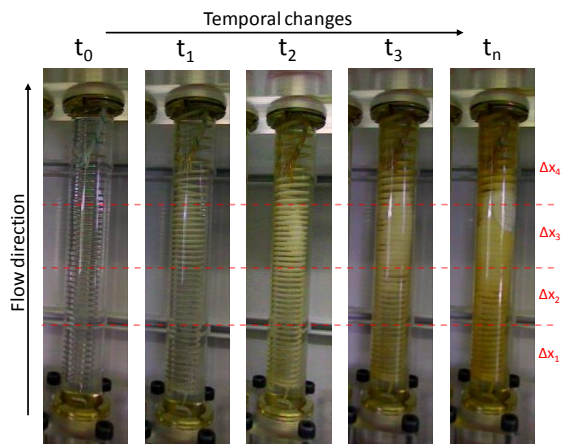
Fig. 13. Time-dependent images of a contaminated bare-wire heating element in test series NE2: t_0 - clean surface, t_1 - partly covered surface with deposited crystal layer, t_2 - entirely covered surface with deposited crystal layer, t_3 - highly soiled wire with partly covered coil pitches in segment Δx_3 and Δx_4, t_n - very highly soiled wire just before the heating element fails

At the beginning of the duration test, no deposition is observed, as shown in Fig. 13 (t_0). In the flow direction, the fluid temperature is increased by the bare-wire heating element. Therefore, it is detected that the deposited crystal layer thickness is greater in segments Δx_3 and Δx_4 than in segments Δx_1 and Δx_2, as can be observed in Fig. 13 (t_1). This can also be observed at each time-dependent image in Fig.

13. It can be assumed that the first nucleation and crystal growth begin at segment Δx_4 because of the highest surface and fluid temperatures. This is confirmed in Fig. 13 (t_2). Additionally, it is identified that the first covered coil pitches are seen in segment Δx_3. In Fig. 13 (t_3), it is observed that the fouling layer has grown further in all the segments. Fig. 13 (t_n) shows the fouling distribution just before the heating element fails. At this time, it is shown that large parts of coil pitches in segments Δx_2, Δx_3, and Δx_4 are covered with a deposited fouling layer over the coil circumference. Similar fouling stages are detected during the execution of test series NE1 and NE3; the observation in segment Δx_4 is presented in Fig. 14.
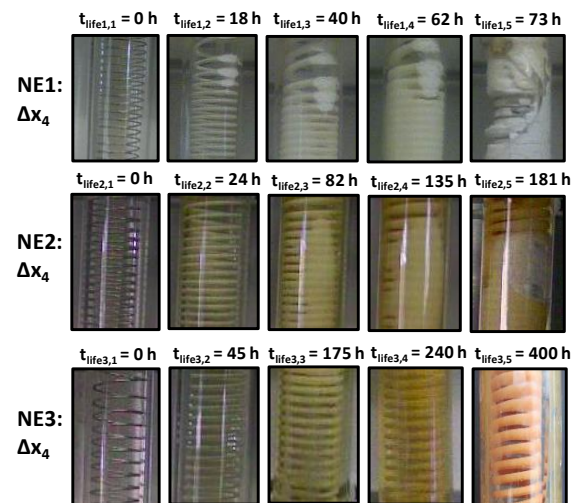
Fig. 14. Comparison of time-dependent images of contaminated bare-wire heating elements in segment Δx_4 in test series NE1, NE2, and NE3

In all the test series, the fouling distribution is similar over the heating length and along the flow direction until the bare-wire heating element fails. In all observed tests, an increase in the flowrate causes an extended lifetime as explained above. Furthermore, a critical point can be observed when the coil pitches are covered with a crystal layer over a large part of the coil. Subsequently, the local fouling tendency is favored because the flow conditions are changed. In addition, the fouling layer grows in the wall direction faster than in the bulk flow direction and changed the free-flow cross-section. Therefore, the high effective shear stresses result from the constriction of the free-flow cross-section in this area and influence the flow conditions. Under clean surface conditions, bare-wire heating elements show a dynamic turbulence flow behavior owing to the properties of the coil geometry, as explained by Gusig [1]. Time-dependent deposition initially changes the flow condition of a coil flow to a circular ring flow and finally to a pipe flow. These flow conditions, which are dependent on the soiled heating element conditions, result in a reduction in the heat transfer and therefore in the lifetime of the bare-wire heating

elements. Based on these findings, a schematic of local and temporal fouling deposits on the bare-wire heating elements was derived, as illustrated in Fig. 15.
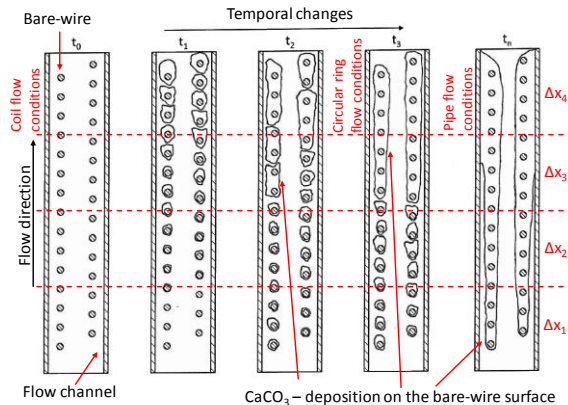
Fig. 15. Derivation of different stages of local and temporal fouling deposition on bare-wire heating elements in section A–A

Local fouling layer thickness and morphology of $CaCO_3$ fouling deposits

Fig. 16 shows the determined local fouling thickness over the tube length of the tested bare-wire heating elements and illustrates its dependence on flowrates.
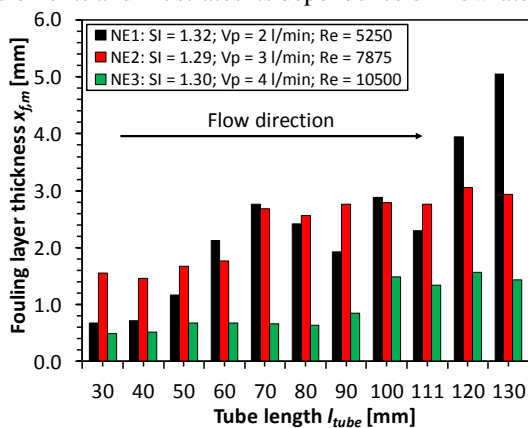
Fig. 16. Average local thickness of the fouling layers as a result of the optical analysis in test series NE1, NE2, and NE3

It can be observed in Fig. 16 that, in the flow direction, the fouling thickness increases. A significant increase in the fouling layer thickness was found between the section at 100 mm to 130 mm in the case of all the test series. Fig. 16 also shows that the fouling thickness sometimes slowly decreases, as observed in the section between 70 mm to 90 mm in the test series NE1. During the test period, parts of the forming crystal deposits were completely removed or partly peeled off. Thus, the fouling thicknesses varies over the tube length. For the used bare-wire heating elements, it can be assumed that for the fouling thickness of 0.85 mm (half of coil pitch $a_w = 1.69$ mm), the heat transfer significantly decreases because the coil pitches are covered by crystal deposits. This shows that an

increase in the coil pitch could result in an extended lifetime of the bare-wire heating elements.

In addition to the previous optical analysis, light microscope images of the fouling layer morphology were analyzed to understand the heat transfer during the local crystal growth of bare-wire heating elements. Fig. 17 shows some examples of typical morphology structures.
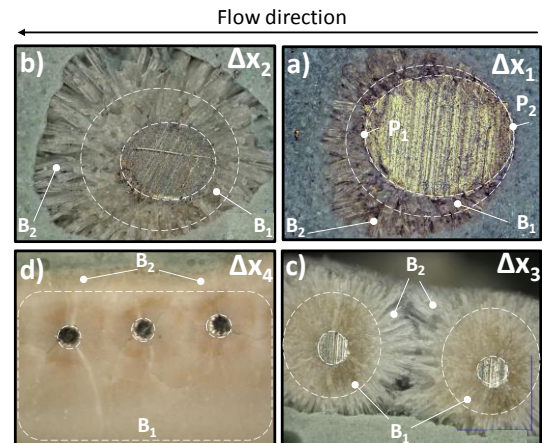
Fig. 17. Typical morphology structures at different stages and cross-sections on bare-wire heating elements: first grown fouling layer (a); completely formed crystal layer over wire circumference (b); well-formed crystal layer with covered coil pitch (c); compact formed crystal layer with completely enclosed coil pitches (d)

The crystal layer growth on a bare-wire surface can be divided into two areas as illustrated in Figs. 7 and 17: the compact crystal layer area B_1 and the crystal needles area B_2. At the beginning of the crystal growth over the bare-wire circumference, no deposits are observed at position P_2 as observed in Fig. 17a. The first crystal growth starts at position P_1, and the base layer grows from that point to the flow direction. In Fig. 17b, a circumferential fouling layer along the wire circumference is shown. This fouling layer increases the thermal conduction resistance and reduces the direct convective heat transfer. However, Fig. 17b additionally shows well-formed crystal needles in area B_2, which leads to an increase in the surface roughness on the compact crystal layer B_1, and therefore, to an improvement in the local heat transfer coefficient due to a higher turbulence. The next fouling stage is illustrated in Fig. 17c. It shows a compact core layer B_1 and well-oriented crystal needles B_2, which grow thicker and longer in this stage. Furthermore, the mesh of needles is interlocked more densely between the coil pitch. Thus, the local heat transfer between the two wires is further reduced because of the covered coil pitch. In this stage, the thermal conduction resistance of the compact fouling layer B_1 is often larger than the improved heat transfer by the increased fluid velocity owing to the reduced free-flow cross-section. Fig. 17d presents a visualization of the final stage of the local fouling morphology on bare-wire heating elements before

they fail. The deposits enclosed some coil pitches completely. This deposited compact fouling layer B_1 is packed hard and more densely over the operating time. The heat transfer of the bare-wire heating element is essentially driven by the heat conduction and less by the heat convection in this stage. Thus, the heating element is not cooled sufficiently, and it overheats over time. Immediately, a compact fouling layer is formed, which results in a decrease in the heat-transfer coefficient, and therefore, to an increase in the fouling resistance as observed during the end-life period A_3 in the test series NE1 and NE2.

CONCLUSIONS

In this work, fouling behavior of bare-wire heating elements was investigated. The typical $CaCO_3$ fouling behavior of bare-wire heating elements was determined using the measured fouling resistance at various flowrates. Thereby, a characteristic period was identified, which is characterized by a suddenly increased fouling resistance; it is called the end-life period. The end of this period results in a failure of a bare-wire heating element. Furthermore, it was shown that the lifetime of the bare-wire heating elements is extended when the flowrate is increased. The swinging bare-wire in the flowing fluid contributed to an increase in the lifetime of bare-wire. This phenomenon is observed in the case of a flowrate of 4 l/min. If the effect of the swinging bare-wire increases the turbulence, it results in an enhancement of the heat transfer and reduction of the fouling growth. A unique feature was identified during the optical investigations of the local and temporal crystal growth. Over the operating time, the coil pitches have been completely covered, and a hard and more densely fouling layer was formed. Therefore, different flow conditions were observed during the lifetime of the soiled bare-wire heating elements. These soiling-dependent flow conditions cause a reduction in the heat transfer and, therefore, a reduction in the lifetime of bare-wire heating elements. This observation is based on the assumption that an increase in the coil pitch could extend the lifetime of bare-wire heating elements. An analysis of the crystal morphology showed two essential areas: the compact crystal layer area and the crystal needles area. Both these areas influence the heat transfer in different ways, which necessitates a closer investigation. The findings of the present work can be used to design enhanced bare-wire heating elements with improved durability to crystallization fouling, e.g., increasing coil pitches and reducing flow channel diameter.

NOMENCLATURE

IAP   Ion activity product, $mol^2\,m^{-6}$
J_f Fouling mass flux, $kg\,m^{-2}\,s^{-1}$
J_D Deposition mass flux, $kg\,m^{-2}\,s^{-1}$
J_r Removal mass flux, $kg\,m^{-2}\,s^{-1}$

k   Overall Heat transfer coefficient, $W\,m^{-2}\,K^{-1}$
K_L Solubility product constant, $mol^2\,m^{-6}$
n   Number of measurements, dimensionless
p   Pressure, bar
$\dot{q}$ Heat flux, $W\,cm^{-2}$
R_f Fouling resistance, $cm^2\,K\,W^{-1}$
SI   Saturation index, dimensionless
T   Temperature, °C
t   Time, s
x_f Fouling layer thickness, m
$x_{f,m}$ Average fouling layer thickness, m

Greek symbols
Δx Distance, m
λ Thermal conductivity, $W\,m^{-1}\,K^{-1}$
ρ Density, $kg\,m^{-3}$

Subscripts
0   Initial clean condition
el   Electrical
f   Fouling
fl   Fluid
s   Surface

REFERENCES

[1] Gusig, L.O., *Das stationäre und instationäre Temperaturverhalten von Heizsystemen zur elektrischen Warmwasserbereitung*, Dissertation, Universität Hannover, 1999

[2] Gusig, L.O.; Schmitz E., *The transient thermal response of conventional and new ceramic electrical heating elements under forced convection,* Industrial furnaces and boilers. European Conference No5, Espinho-Porto, Portugal 2000

[3] Epstein, N., *Thinking about heat transfer fouling,* A 5x5 matrix, Heat Trans. Eng., Vol. 4, pp. 43-56, 1984

[4] Müller-Steinhagen, H., *Cooling-water fouling in heat exchangers*, Adv. Heat Trans., Vol. 33, pp. 415-496, 1999

[5] Steinhagen, H., *Handbook of Heat Exchanger Fouling*, IChemE, Warwickshire, UK 2000

[6] Krause, S., *Fouling of heat-transfer surfaces by crystallization and sedimentation*, Int. Chem. Eng. 33, 3, 1993

[7] Hirsch, H.; Augustin, W.; Bohnet, M., *Influence of fouling layer shear strength on removal behavior*, in Understanding Heat Exchanger Fouling and its Mitigation, eds. T.R. Bott et al., Begell House, New York, p. 201-208, 1999

[8] Wisotzky, F., *Angewandte Grundwasserchemie, Hydrogeologie und hydrogeochemische Modellierung – Grundlagen, Anwendungen und Problemlösungen*, Springer-Verlag Berlin Heidelberg 2011

[9] Förster, M. L., *Verminderung des Kristallisationsfoulings durch gezielte Beeinflussung der Grenzfläche zwischen Kristallen und Wärmeübertragungsflächen*, Dissertation; TU Braunschweig 2001

[10] Geddert, T., *Einfluss von Oberflächenmodifikationen auf die Induktionszeit beim Kristallisationsfouling*, Scholl, S, Augustin, W. (Eds.), ICTV – Schriftreihe Band 6, Cuvillier, Göttingen 2009

[11] Albert, F., *Grenzflächeneffekte bei der kristallinen Belagbildung auf wärmeübertragenden Flächen*, Dissertation, TU Braunschweig 2010

[12] Parkhurst, D., Appelo, C.A.J., *Description of Input and Examples for PHREEQC Version 3,* U.S. Geological Survey Techniques and Methods, book 6, chap. A43, 497 p., available only at http://pubs.usgs.gov/tm/06/a43/; 2013

[13] Augustin, W. and Bohnet, M., *Modelierung des Foulingverhaltens von rauhen Wärmetauscherrohren*, Chem. Ing. Tech., Vol. 66, no. 10, pp. 1396-1399, 1994

[14] Schlüter, F., Schnöing, L., Zettler, H., Augustin, W. and Scholl, S., *Measuring local crystallization fouling in a double-pipe heat exchanger*, Heat exchanger fouling and cleaning conference 2017